LETTERS
https://doi.org/10.1038/s41558-018-0361-0
nature climate change

Hydrologic implications of vegetation response to elevated CO_2 in climate projections

Yuting Yang[1,2,6*], Michael L. Roderick[1,2,3*], Shulei Zhang[4], Tim R. McVicar[2,5] and Randall J. Donohue[2,5]

Climate model projections using offline aridity and/or drought indices predict substantial terrestrial drying over the twenty-first century[1–11]. However, these same models also predict an increased runoff[12–15]. This contradiction has been linked to an absence of vegetation responses to an elevated atmospheric CO_2 concentration [CO_2] in offline impact models[12,14,16,17]. Here we report a close and consistent relationship between changes in surface resistance (r_s) and [CO_2] across 16 CMIP5 models. Attributing evapotranspiration changes under non-water-limited conditions shows that an increase in evapotranspiration caused by a warming-induced vapour pressure deficit increase[18] is almost entirely offset by a decrease in evapotranspiration caused by increased r_s driven by rising [CO_2]. This indicates that climate models do not actually project increased vegetation water use under an elevated [CO_2], which counters the perception that 'warming leads to drying' in many previous studies[1–11]. Moreover, we show that the hydrologic information in CMIP5 models can be satisfactorily recovered using an offline hydrologic model that incorporates the [CO_2] effect on r_s in calculating potential evapotranspiration (E_P). This offers an effective, physically-based yet relatively simple way to account for the vegetation response to elevated [CO_2] in offline impact models.

The response of terrestrial water availability (and thus aridity and drought) to future climate change is a key concern in the hydrologic and related scientific communities, and for society in general. From a hydrologic perspective, over long periods and without direct human interventions, terrestrial water availability can be represented as a functional balance between precipitation (P) and potential evapotranspiration[19] (E_P, the rate of evapotranspiration when the surface is not water stressed[12]). Although P is an observable variable and a direct climate model output, E_P is often neither observable nor directly used (or produced) by climate models. Consequently, in assessing climate model projections, an E_P model is required beforehand to estimate E_P based on climate model outputs of meteorological variables. The estimated E_P is then applied in various offline aridity indices[3–6,10], drought indices[1,2,9,11] and hydrologic models[20] to assess aridity and/or drought changes.

Among numerous E_P algorithms, the Penman–Monteith-type models explicitly consider influences from both radiative and aerodynamic components and are regarded as an accurate yet simple approximation to the more complex system embedded in climate models[12]. As such, two variants of the original Penman–Monteith model, that is, the open-water Penman model (Penman-OW)[21] and the reference crop Penman–Monteith model (PM-RC)[22], are the most widely used to estimate E_P in existing studies of change and/or impact models that include aridity and/or drought[1–7,11,23]. Based on E_P estimates from these two models and climate projections from the Coupled Model Intercomparison Project Phase 5 (CMIP5) models, many studies have concluded a substantial drying trend over global terrestrial environments towards the end of the twenty-first century according to offline calculated aridity and/or drought indices[1–11]. However, this twenty-first century drying trend based on aridity and drought indices contradicts with direct CMIP5 model outputs of increases in runoff[13–17], which suggests a reduction in the future aridity in many regions. This implies that those offline aridity/drought assessments do not faithfully represent the physical and/or biological processes in CMIP5 models[12,14]. Recent studies argue that such a contradiction is partly due to ignoring the increased r_s over vegetated lands induced by an elevated atmospheric [CO_2] (refs. [12,14,16,17]). In Penman-OW, which was designed for water surfaces, r_s is fixed at zero;[21] and in PM-RC, r_s is set to a constant value of 70 s m^{-1}, which is appropriate for an idealized reference crop in the current climate[22]. To neglect the increase of r_s under an elevated [CO_2] would thus overestimate the future drying trend[12–14,16,17]. In this light, it is necessary to incorporate the response of r_s to an elevated [CO_2] in the calculation of E_P so that we can better recover the hydrologic information from climate model output and hence obtain more meaningful assessments of changes and impacts of future aridity/drought that more faithfully represent the CMIP5 models.

Here we examine long-term changes in r_s and its relationship to changes in atmospheric [CO_2] in 16 CMIP5 models (Supplementary Table 1) under historical (1861–2005) and Representative Concentration Pathway 8.5 (RCP8.5; 2006–2100) experiments. The numerical value of r_s in climate model output is obtained by inverting the Penman-Monteith model with climate model outputs of actual evapotranspiration (E) and other meteorological forcing variables. To focus on the impact of elevated [CO_2] on r_s and E_P, we only examined r_s in regions and/or months for each of the 16 CMIP5 models when E is not water limited[12] (Methods and Supplementary Fig. 1). Following Milly and Dunne[12], we also limited our analyses to regions/months when the monthly mean air temperature is higher than 10 °C, to avoid uncertainties caused by frozen water.

Averaged over 16 CMIP5 models and across all non-water-limited regions and/or months, the change in r_s (Δr_s) exhibits a very

[1]Research School of Earth Sciences, Australian National University, Canberra, ACT, Australia. [2]Australian Research Council Centre of Excellence for Climate System Science, Canberra, ACT, Australia. [3]Australian Research Council Centre of Excellence for Climate Extremes, Canberra, ACT, Australia. [4]State Key Laboratory of Hydroscience and Engineering, Department of Hydraulic Engineering, Tsinghua University, Beijing, China. [5]CSIRO Land and Water, Black Mountain, Canberra, ACT, Australia. [6]Present address: State Key Laboratory of Hydroscience and Engineering, Department of Hydraulic Engineering, Tsinghua University, Beijing, China. *e-mail: yuting_yang@tsinghua.edu.cn; michael.roderick@anu.edu.au

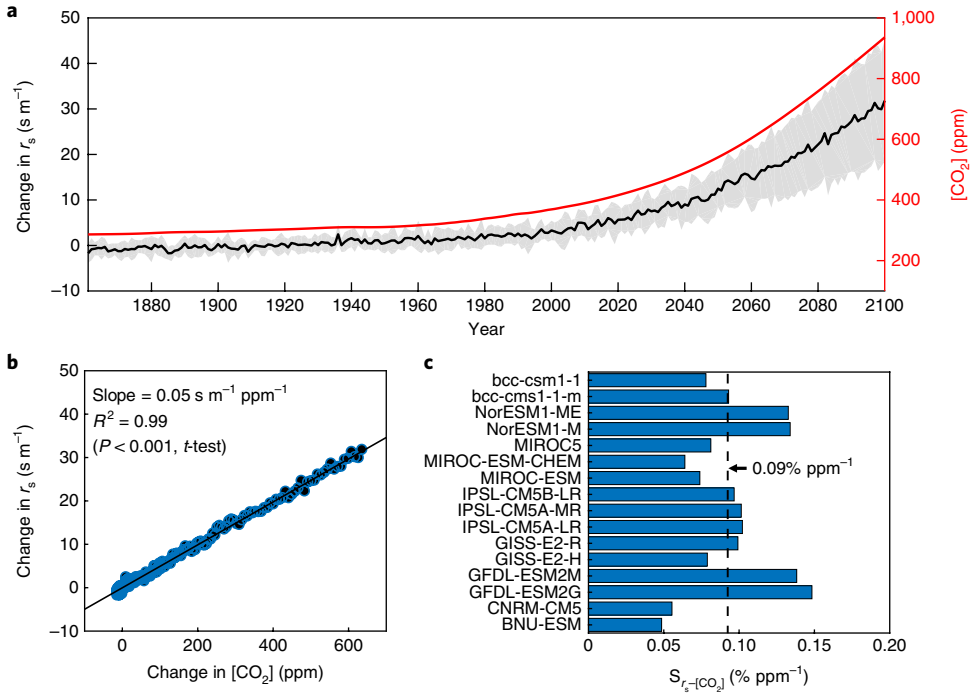

Fig. 1 | Changes in r_s over non-water-limited regions and/or months under elevated atmospheric [CO$_2$]. a, Changes in annual mean r_s relative to the 1861–1960 baseline in 16 CMIP5 models. The black curve indicates the ensemble mean of 16 CMIP5 models and the shaded area represents ±1 s.d. among the models. The red curve is the atmospheric [CO$_2$]. **b**, Relationship between the ensemble mean of changes in r_s and [CO$_2$] (relative to the 1861–1960 baseline). **c**, Sensitivity of r_s to [CO$_2$] for 16 CMIP5 models (that is, % change in r_s per ppm increase in [CO$_2$]). The vertical dashed black line indicates the ensemble mean of 16 CMIP5 models.

close linear relationship with the change in atmospheric [CO$_2$] (Δ[CO$_2$]) during 1861–2100 (Fig. 1a,b). The mean value of r_s increases from ~55 s m^{-1} when [CO$_2$] is ~300 ppm in the 1861–1960 historical period to ~80 s m^{-1} when [CO$_2$] is ~807 ppm in the 2071–2100 future period (Supplementary Fig. 2), which indicates a 25 s m^{-1} (or ~45%) increase in r_s for a 507 ppm (or ~169%) increase in [CO$_2$]. The linear relationship between Δr_s and Δ[CO$_2$] is consistent across all 16 CMIP5 models, with R^2 of a linear-fit function between Δr_s and Δ[CO$_2$] ranging from 0.75 to 0.99 across models (Supplementary Fig. 3). More importantly, the relative sensitivity of r_s to Δ[CO$_2$] ($S_{r_s-CO_2}$ (Methods)) remains the same order of magnitude across all models (~0.09% ppm^{-1} at 300 ppm (Fig. 1c)) and across space (Supplementary Fig. 4), which suggests a uniform r_s response to elevated [CO$_2$] in CMIP5 models.

These results demonstrate for the CMIP5 model output that the implied r_s under non-water-limited conditions is neither zero nor a fixed value of 70 s m^{-1}; instead, r_s steadily increases with atmospheric [CO$_2$]. With a very small mean change in the leaf area index across non-water-limited regions and/or months (Supplementary Fig. 5), this positive Δr_s–Δ[CO$_2$] relationship is primarily caused by the leaf-level response to elevated [CO$_2$] through both direct and indirect pathways. Directly, a higher [CO$_2$] drives partial stomatal closure and consequently indirectly increases r_s (ref. [24]), and, indirectly, the climate response to elevated [CO$_2$] leads to a higher atmospheric vapour pressure deficit (D) that also reduces the stomatal opening[25]. Here we combine these pathways and explore a single relationship between Δr_s and Δ[CO$_2$] as an increased D is ultimately also driven by elevated [CO$_2$] in the CMIP5 RCP8.5 experiment. Our finding confirms previous suggestions[12,14,16,17] that ignoring r_s changes in both PM-RC and Penman-OW in the offline calculated aridity/drought indices[1–7,10] will overestimate changes in E under non-water-limited (E_{NWL}) conditions. Somewhat surprisingly, previous studies found that changes in E_{NWL} only follow changes in surface available energy (R_n*, that is, net radiation minus ground heat flux (W m^{-2})) in CMIP5 model projections, with the aerodynamic components playing a minor role in the control of E_{NWL} changes[12]. To understand further the impact of Δr_s on ΔE_{NWL} and the reasons that underpin a direct ΔE_{NWL}–ΔR_n* relationship, we attribute ΔE_{NWL} to different forcing factors based on the original Penman–Monteith model (Methods). Averaged over all non-water-limited regions/months and across 16 CMIP5 models, E_{NWL} increases from 3.87 mm day^{-1} (1861–1960) to 4.01 mm day^{-1} (2071–2100) (or by +0.14 mm day^{-1} or +3.6%) (Fig. 2a). For the same period, changes in R_n*, D, r_s, aerodynamic resistance (r_a) and the saturated vapour pressure versus temperature slope (s), respectively, lead to changes in E_{NWL} of +0.11 mm day^{-1} (+2.8%), +0.33 mm day^{-1} (+8.5%), −0.31 mm day^{-1} (−8.1%), +0.005 mm day^{-1} (+0.1%) and −0.0004 mm day^{-1} (−0.01%). This indicates that the ΔD-induced increase in E_{NWL} and Δr_s-induced decrease in E_{NWL} effectively cancel. With very small changes in E_{NWL} induced by both Δr_a (driven by wind speed changes for a fixed vegetation height) and Δs, it follows that the overall change in E_{NWL} more or less follows the change in R_n*. More interestingly, we find that the cancellation between ΔD-induced ΔE_{NWL} and Δr_s-induced ΔE_{NWL} is common across each individual CMIP5 model considered here (Fig. 2b,c, and Supplementary Fig. 6). Note that the CMIP5 models do not use the Penman-Monteith formulation to calculate E. Hence, our finding that the positive impact of an increased D (primarily driven by warming[18]) on E_{NWL} is more or less cancelled by a negative impact of the increased r_s (driven by elevated [CO$_2$] and D) on E_{NWL} suggests this must be a common corollary that emerges from the non-linear system of equations that are solved in CMIP5 models. This finding further demonstrates why warming does not necessarily lead to an increased E in a [CO$_2$]-enriched environment, which refutes the perception that "warming leads to drying", which commonly exists in the literature[1–11].

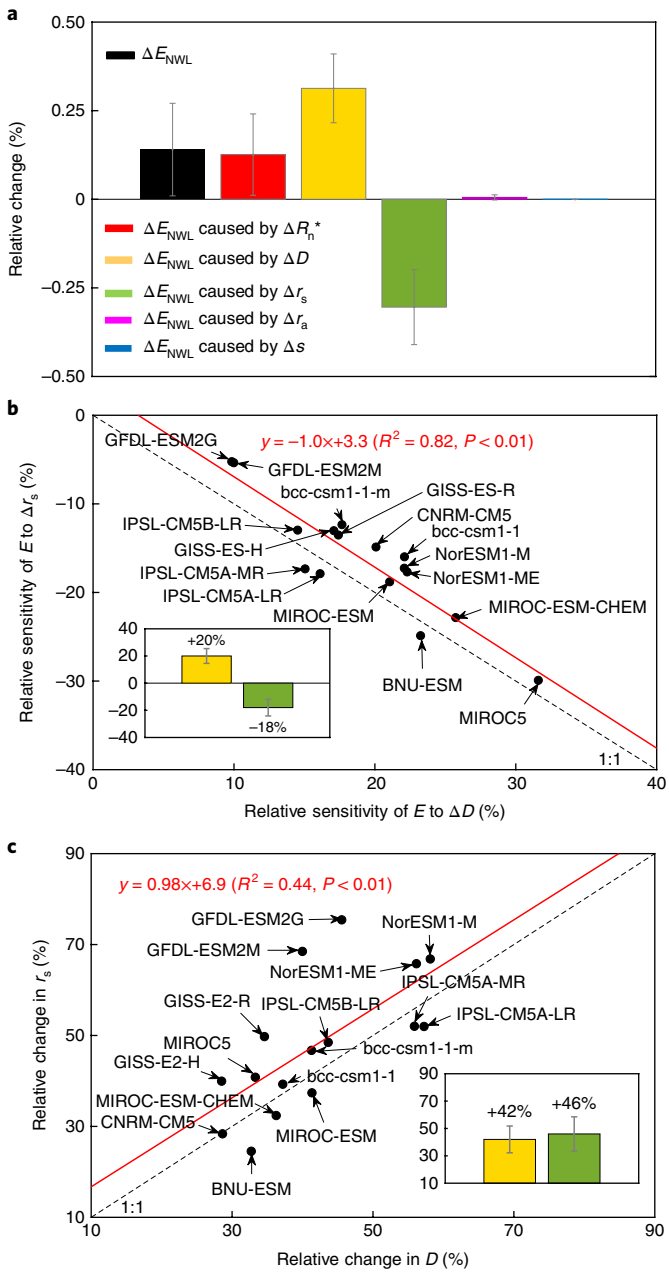

Fig. 2 | Attribution of change in E_{NWL}. **a**, Attribution of change in E_{NWL} between 2071–2100 and 1861–1960. Bars and error bars represent the ensemble mean and ±1 s.d. over 16 CMIP5 models, respectively. **b**, Relationship between relative sensitivity of E to changes in D ($S_{E\text{-}D}$) and r_s (S_{E-r_s}) over non-water-limited regions and/months for 16 CMIP5 models. **c**, Relationship between relative changes in r_s and D (period 2071–2100 compared to period 1861–1960) over non-water-limited regions and/or months for 16 CMIP5 models. Insets, ensemble mean (bars) and ±1 s.d. (error bars) over 16 CMIP5 models.

The conservative response reported here across all 16 CMIP5 models (Figs. 1 and 2) suggests a simple approach can be used to account for the impact of atmospheric $[CO_2]$ changes on r_s under non-water-limited conditions in the Penman–Monteith model. For that, we explicitly express r_s as a function of $[CO_2]$ (in ppm):

$$r_s([CO_2]) = r_{s-300} \times \{1 + S_{r_s-[CO_2]} \times ([CO_2] - 300)\} \quad (1)$$

where r_{s-300} is the reference surface resistance when atmospheric $[CO_2]$ is 300 ppm (roughly equivalent to the 1861–1960 mean), and $S_{r_s-CO_2}$ is the relative sensitivity of r_s to $\Delta[CO_2]$. In the ensemble of CMIP5 models, r_{s-300} is ~55 s m^{-1} and $S_{r_s-CO_2}$ is ~0.09 % ppm^{-1} (Fig. 1b,c). Combining equation (1) with the Penman–Monteith model (that is, equation (3) in Methods) gives a new method for calculating E_P (referred to here as PM-$[CO_2]$) that explicitly accounts for the effects of an elevated $[CO_2]$ (Methods).

To examine the hydrologic implications of different E_P formulations, we compared the estimated runoff changes (ΔQ, relative to the 1861–1960 baseline) from a widely used and transparent model (the Budyko hydro-climatological model) forced with different E_P estimates against ΔQ directly simulated by the CMIP5 models (Methods). Compared with the direct CMIP5 model projections, the Budyko model substantially underestimates ΔQ (and overestimates ΔE) when forced with E_P estimates from both PM-RC and Penman-OW (Fig. 3a and Supplementary Fig. 7). Averaged over all global land (excluding Greenland and Antarctica), the ensemble CMIP5 models project an increased Q of +36 mm yr^{-1} in the future period 2071–2100 relative to the historical period 1861–1960. However, when the Budyko model is forced with PM-RC and Penman-OW the ΔQ is +8 mm yr^{-1} and +6 mm yr^{-1}, respectively (Fig. 3a). Larger underestimates are generally found in relatively humid areas (for example, Amazonia, Europe, Central America and southeast Asia), where Q is large and most sensitive to E_P (ref. [19]) (Fig. 3b–d). In contrast, the Budyko model forced with PM-$[CO_2]$ performed much better in reproducing ΔQ simulated by the CMIP5 model, in terms of both magnitude (ΔQ from Budyko forced with PM-$[CO_2]$ is +32 mm yr^{-1}) and spatial pattern (Fig. 3). However, a slight discrepancy of ΔQ (Fig. 3b–e) is still present, which may be caused by ignoring other factors that are not explicitly included in the Budyko model, such as changes in rainfall intensity[26], climate seasonality[27] and/or leaf area index (leaf area index increases are more common in cold/temperate regions and in dry regions (Supplementary Fig. 5)). Nevertheless, our use of PM-$[CO_2]$ reduced the global mean ΔQ estimation bias from ~30 mm yr^{-1} to 4 mm yr^{-1} and demonstrates a dramatic improvement in the recovery of hydrologic information from CMIP5 models due to including the response of r_s to elevated atmospheric $[CO_2]$.

Although it is a common practice to assess future hydrologic changes (for example, aridity and drought) in climate model projections by using offline impact models, a scientific prior is that the adopted offline impact models should be able to reproduce the hydrologic information in the climate model output[16]. This is because the climate models are fully coupled land (and ocean)–atmosphere models that are internally consistent (yet imperfect) representations of the climate system[12]. This implies that any inconsistency of hydrologic predictions between offline impact models and climate models themselves would lead to inconsistent predictions in other aspects of the climate system (for example, a higher E_P and thus E would lead to a lower surface temperature). Here we demonstrate that the hydrologic changes in CMIP5 models can be satisfactorily recovered by explicitly considering the response of r_s to elevated atmospheric $[CO_2]$ in the calculation of E_P and an offline impact model. In this light, the PM-$[CO_2]$ model proposed herein can be used as a standard method that can recover the climate model output in a changing $[CO_2]$ environment.

Note that our findings are based on CMIP5 model outputs. Whether and to what extent equation (1) could represent the real world remains an open question for future investigations. Based on a synthesis of 244 field observations on the stomatal response to elevated atmospheric $[CO_2]$ across global bioclimates, Ainsworth and Rogers[28] reported a mean reduction in leaf-level stomatal conductance of 22% for an increase in $[CO_2]$ of 201 ppm (from 366 to 567 ppm). This is equivalent to a stomatal resistance sensitivity to $\Delta[CO_2]$ of 0.11% ppm^{-1}. To convert that into an estimate of r_s sensitivity, we have to account for the fraction of E represented by transpiration. Adopting a global average transpiration/E ratio of

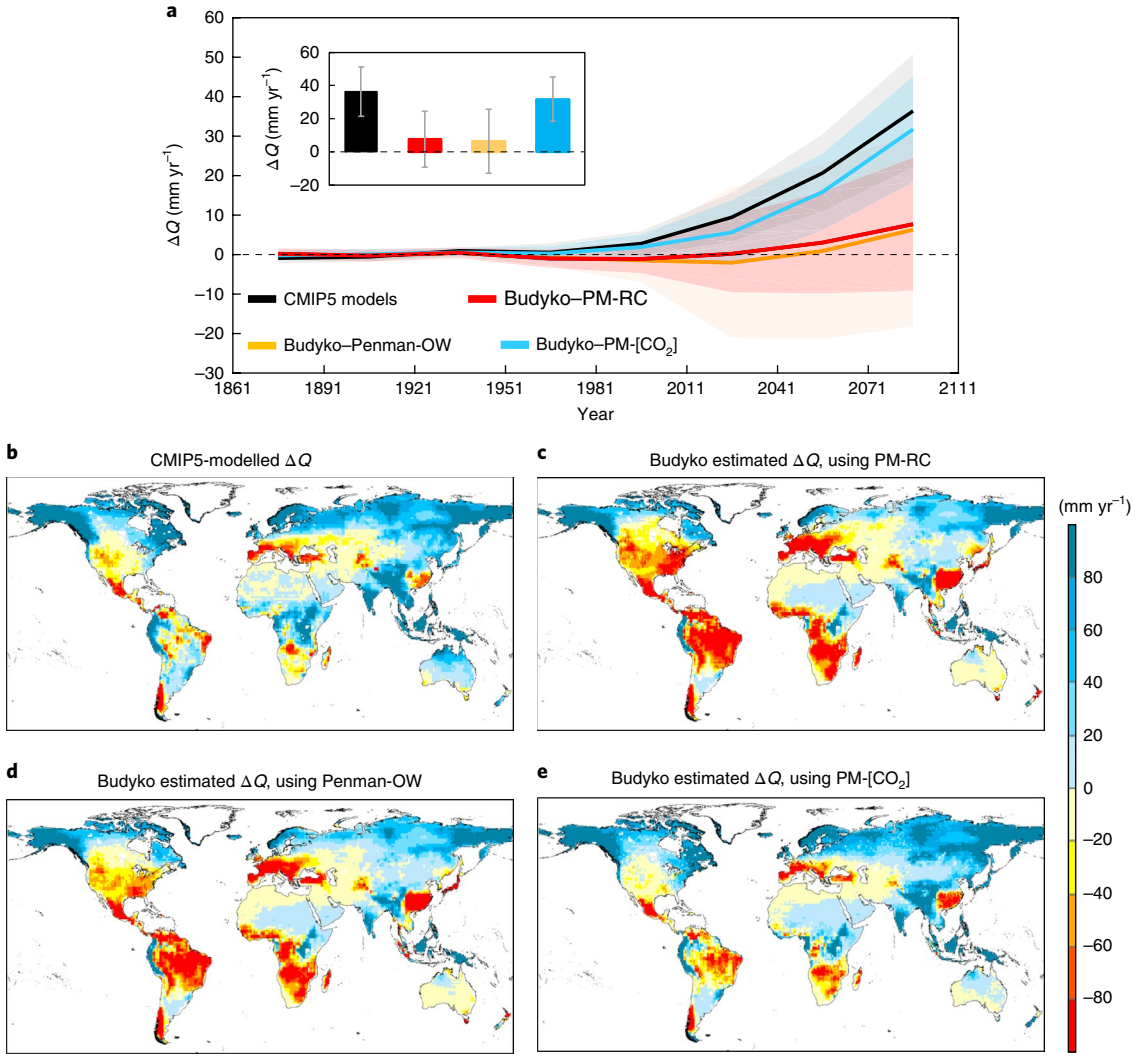

Fig. 3 | Changes in modelled runoff in the future period 2071–2100 relative to the historic period 1861–1960. a, Sequential 30 yr mean annual ΔQ over 1861–2100 compared to the 1861–1960 baseline estimated by four methods, including the direct CMIP5 model output (black), the Budyko model forced with PM-RC, Penman-OW and PM-[CO_2] (equation (1)). The solid curves are the ensemble mean of 16 CMIP5 models and the shading represents ±1 s.d. among 16 CMIP5 models. Inset, ensemble mean of ΔQ between 2071–2100 and 1861–1960, with error bars illustrating ±1 s.d. **b**–**e**, Spatial distribution of the modelled mean annual ΔQ between 2071–2100 and 1861–1960 from the four methods.

70% (that is, the mid-value within a typical reported range of 60%–80% (refs. [29,30])), we estimate a relative sensitivity of r_s to $\Delta[CO_2]$ of ~0.08% ppm^{-1}. This is almost identical to the estimate we obtained from the ensemble of 16 CMIP5 models (that is, 0.09% ppm^{-1} (Fig. 1c)), which suggests that equation (1) might also be widely applicable to real-world conditions.

Online content

Any methods, additional references, Nature Research reporting summaries, source data, statements of data availability and associated accession codes are available at https://doi.org/10.1038/s41558-018-0361-0.

Received: 18 April 2018; Accepted: 14 November 2018;
Published online: 17 December 2018

References

1. Cook, B. I., Smerdon, J. E., Seager, R. & Coats, S. Global warming and 21st century drying. *Clim. Dynam.* **43**, 2607–2627 (2014).
2. Dai, A. Increasing drought under global warming in observations and models. *Nat. Clim. Change* **3**, 52–58 (2012).
3. Feng, S. & Fu, Q. Expansion of global drylands under a warming climate. *Atmos. Chem. Phys.* **13**, 10081–10094 (2013).
4. Fu, Q. & Feng, S. Responses of terrestrial aridity to global warming. *J. Geophys. Res. Atmos.* **119**, 7863–7875 (2014).
5. Huang, J., Yu, H., Guan, X., Wang, G. & Guo, R. Accelerated dryland expansion under climate change. *Nat. Clim. Change* **6**, 166–171 (2015).
6. Lin, L., Gettelman, A., Feng, S. & Fu, Q. Simulated climatology and evolution of aridity in the 21st century. *J. Geophys. Res. Atmos.* **120**, 5795–5815 (2015).
7. Park, C.-E. et al. Keeping global warming within 1.5 °C constrains emergence of aridification. *Nat. Clim. Change* **8**, 70–74 (2018).
8. Sherwood, S. & Fu, Q. A drier future? *Science* **343**, 737–739 (2014).
9. Trenberth, K. E. et al. Global warming and changes in drought. *Nat. Clim. Change* **4**, 17–22 (2013).
10. Scheff, J. & Frierson, D. M. W. Terrestrial aridity and its response to greenhouse warming across CMIP5 climate models. *J. Clim.* **28**, 5583–5600 (2015).
11. Naumann, G. et al. Global changes in drought conditions under different levels of warming. *Geophys. Res. Lett.* **45**, 3285–3296 (2018).
12. Milly, P. C. D. & Dunne, K. A. Potential evapotranspiration and continental drying. *Nat. Clim. Change* **6**, 946–949 (2016).
13. Greve, P., Roderick, M. L. & Seneviratne, S. I. Simulated changes in aridity from the last glacial maximum to 4xCO_2. *Environ. Res. Lett.* **12**, 114021 (2017).
14. Roderick, M. L., Greve, P. & Farquhar, G. D. On the assessment of aridity with changes in atmospheric CO_2. *Water Resour. Res.* **51**, 5450–5463 (2015).

15. Scheff, J., Seager, R., Liu, H. & Coats, S. Are glacials dry? Consequences for paleoclimatology and for greenhouse warming. *J. Clim.* **30**, 6593–6609 (2017).
16. Milly, P. C. D. & Dunne, K. A. A hydrologic drying bias in water-resource impact analyses of anthropogenic climate change. *J. Am. Water Resour. Assoc.* **53**, 822–838 (2017).
17. Swann, A. L. S., Hoffman, F. M., Koven, C. D. & Randerson, J. T. Plant responses to increasing CO_2 reduce estimates of climate impacts on drought severity. *Proc. Natl Acad. Sci. USA* **113**, 10019–10024 (2016).
18. Scheff, J. & Frierson, D. M. W. Scaling potential evapotranspiration with greenhouse warming. *J. Clim.* **27**, 1539–1558 (2014).
19. Roderick, M. L., Sun, F., Lim, W. H. & Farquhar, G. D. A general framework for understanding the response of the water cycle to global warming over land and ocean. *Hydrol. Earth Syst. Sci.* **18**, 1575–1589 (2014).
20. Samaniego, L. et al. Anthropogenic warming exacerbates European soil moisture droughts. *Nat. Clim. Change* **8**, 421–426 (2018).
21. Shuttleworth, W. J. in *Handbook of Hydrology* (ed. Maidment, D. R.) Ch. 4 (McGraw-Hill Education, New York, 1993).
22. Allen, R. G., Pereira, L. S., Raes, D. & Smith, M. *Crop Evapotranspiration—Guidelines for Computing Crop Water Requirements* FAO Irrigation and Drainage Paper No. 56 (FAO, 1998).
23. Sheffield, J., Wood, E. F. & Roderick, M. L. Little change in global drought over the past 60 years. *Nature* **491**, 435–438 (2012).
24. Field, C. B., Jackson, R. B. & Mooney, H. A. Stomatal responses to increased CO_2: implications from the plant to the global scale. *Plant Cell Environ.* **18**, 1214–1225 (1995).
25. Novick, K. A. et al. The increasing importance of atmospheric demand for ecosystem water and carbon fluxes. *Nat. Clim. Change* **6**, 1023–1027 (2016).
26. Westra, S. et al. Future changes to the intensity and frequency of short-duration extreme rainfall. *Rev. Geophys.* **52**, 522–555 (2014).
27. Chou, C. et al. Increase in the range between wet and dry season precipitation. *Nat. Geosci.* **6**, 263–267 (2016).
28. Ainsworth, A. E. & Rogers, A. The response of photosynthesis and stomatal conductance to rising [CO_2]: mechanisms and environmental interactions. *Plant Cell Environ.* **30**, 258–270 (2007).
29. Jasechko, S. et al. Terrestrial water fluxes dominated by transpiration. *Nature* **496**, 347–350 (2013).
30. Zhang, Y. et al. Multi-decadal trends in global terrestrial evapotranspiration and its components. *Sci. Rep.* **6**, 19124 (2016).

Acknowledgements

Y.Y. and M.R. acknowledge the support of the Australian Research Council (CE1101028, CE170100023). T.M. and R.D. acknowledge the support from CSIRO Land and Water.

Author contributions

Y.Y., M.R., T.M. and R.D. conceived the idea. Y.Y. and M.R. designed the study. Y.Y. and S.Z. performed the analyses. Y.Y. drafted the manuscript. All the authors contributed to results, discussion and manuscript writing.

Competing interests

The authors declare no competing interests.

Additional information

Supplementary information is available for this paper at https://doi.org/10.1038/s41558-018-0361-0.

Reprints and permissions information is available at www.nature.com/reprints.

Correspondence and requests for materials should be addressed to Y.Y. or M.L.R.

Publisher's note: Springer Nature remains neutral with regard to jurisdictional claims in published maps and institutional affiliations.

Methods

Climate model projections. We used outputs from 16 climate models that participate in CMIP5 (Supplementary Table 1) under both historical (1861–1960) and a high emission scenario (RCP 8.5) experiments[31]. The selected 16 CMIP5 models all report runoff and all the required meteorological variables. We used monthly outputs of runoff, precipitation, actual evapotranspiration, sensible heat flux and latent heat flux at the land surface, and near-surface air temperature, air pressure, wind speed and specific humidity. All the outputs from the 16 CMIP5 models were resampled to a common 1° spatial resolution by using the first-order conservative remapping scheme[32].

Determining r_s over non-water-limited regions and/or months. To examine the response of r_s to elevated atmospheric [CO_2], we selected regions/months at which evapotranspiration is not limited by water stress[12]. Specifically, for each model, for each sequential 30 yr period during 1861–2100 (leading to eight 30 yr periods) and for each month and grid cell, we fitted the 30 pairs of monthly evapotranspiration and precipitation model outputs with a parabolic function[12]. For each precipitation value, we obtained the slope of the fitted parabola relationship and found the maximum slope among those 30 slopes. The non-water-limited condition for each 30 yr period was defined as regions/months in which the maximum slope was less than 0.05 and the ratio of evapotranspiration over precipitation was less than two[12]. We used the common non-water-limited regions/months for all eight 30 yr periods for each model. To avoid uncertainties caused by frozen water, we also excluded regions/months where the monthly mean air temperature is lower than 10 °C (ref. [12]) (Supplementary Fig. 1). The values of r_s at grid cells that belong to non-water-limited regions/months were quantified by inverting the Penman–Monteith model for each CMIP5 model (that is, equation (3)). The annual mean r_s for each model and each year was then determined by averaging monthly r_s values over all non-water-limited grid cells and months during that year. The relative sensitivity of r_s to Δ[CO_2] is defined as:

$$S_{r_s-CO_2}=\frac{r_s-r_{s-300}}{r_{s-300}}\frac{1}{[CO_2]-300} \quad (2)$$

where $S_{r_s-CO_2}$ is the relative sensitivity of r_s to changes in [CO_2]. r_{s-300} is more or less equivalent to the 1861–1960 mean r_s.

Penman–Monteith model with [CO_2] adjustment. The Penman–Monteith model calculates E as:

$$\lambda E=\frac{sR_n^*+\rho_a C_P D/r_a}{s+\gamma(1+r_s/r_a)} \quad (3)$$

where s is the gradient of the saturation vapour pressure with respect to temperature (Pa K^{-1}), γ is the psychrometric constant (Pa K^{-1}), ρ_a is the air density (kg m^{-3}), C_P is the specific heat of air at constant pressure (J kg^{-1} K^{-1}), u is the wind speed at 2 m height (m s^{-1}), D is the vapour pressure deficit of the air at 2 m height (the difference between the saturated vapour pressure and the actual vapour pressure (Pa)), λ is the latent heat of vaporization (J kg^{-1}), which is calculated as a function of air temperature[12]. r_a (s m^{-1}) is inversely proportional to the wind speed and changes with the surface roughness length[21]. The surface resistance, r_s, is calculated as a function of [CO_2] using equation (1).

Penman-OW E_P model. The Penman-OW model is a simplified version of the Penman–Monteith model over an open-water surface and used to calculate E_P ($r_s=0$ and an aerodynamic roughness of the surface of 0.00137 m). It computes E_P (mm day^{-1}) as[21]:

$$\lambda E_P=\frac{sR_n^*+6.43(1+0.536u)\gamma D}{s+\gamma} \quad (4)$$

PM-RC E_P model. The PM-RC model is another standardized version of the Penman–Monteith model that is applicable to an idealized reference crop surface ($r_s=70$ s m^{-1}, vegetation height of 0.12 m and surface albedo of 0.23). This model calculates E_P (mm day^{-1}) as[22]:

$$E_P=\frac{0.408sR_n^*+\gamma\frac{900}{T+273}uD}{s+\gamma(1+0.34u)} \quad (5)$$

where the available energy R_n^* is given in MJ m^{-2} day^{-1} and T is the air temperature (°C).

Attribution of changes in E. We attribute changes in E to different forcing variables based on the original Penman–Monteith model (that is, equation (3)). As changes in λ are general very small (changes in λ are less than 3% for a temperature range between 10 and 40 °C), we only consider changes in E with respect to the remaining five variables in equation (3) (that is, R_n^*, D, r_s, r_a and s). To the first order, changes in E can be approximated as:

$$\Delta E\approx\frac{\partial E}{\partial R_n^*}\Delta R_n^*+\frac{\partial E}{\partial D}\Delta D+\frac{\partial E}{\partial r_s}\Delta r_s+\frac{\partial E}{\partial r_a}\Delta r_a+\frac{\partial E}{\partial s}\Delta s \quad (6)$$

where the five terms on the right-hand side are ΔE caused by ΔR_n^*, ΔD, Δr_s, Δr_a and Δs, respectively. The partial differentials in equation (6) are given by:

$$\frac{\partial E}{\partial R_n^*}=\frac{s}{\lambda[s+\gamma(1+r_s/e_a)]} \quad (7)$$

$$\frac{\partial E}{\partial D}=\frac{\rho_a C_P}{\lambda r_a[s+\gamma(1+r_s/r_a)]} \quad (8)$$

$$\frac{\partial E}{\partial r_s}=\frac{-\gamma[sR_n^*+\rho_a C_P D/r_a]}{\lambda r_a[s+\gamma(1+r_s/r_a)^2]} \quad (9)$$

$$\frac{\partial E}{\partial r_a}=\frac{\gamma r_s[sR_n^*+\rho_a C_P D/r_a]}{\lambda r_a^2[s+\gamma(1+r_s/r_a)^2]}-\frac{\rho_a C_P D}{\lambda r_a^2[s+\gamma(1+r_s/r_a)]} \quad (10)$$

$$\frac{\partial E}{\partial s}=\frac{R_n^*}{\lambda[s+\gamma(1+r_s/r_a)]}-\frac{R_n^* s+\rho_a C_P D/r_a}{\lambda[s+\gamma(1+r_s/r_a)]^2} \quad (11)$$

The relative change in E is:

$$\frac{\Delta E}{E}\approx\left(\frac{\partial E}{\partial R_n^*}\frac{R_n^*}{E}\right)\frac{\Delta R_n^*}{R_n^*}+\left(\frac{\partial E}{\partial D}\frac{D}{E}\right)\frac{\Delta D}{D}+\left(\frac{\partial E}{\partial r_s}\frac{r_s}{E}\right)\frac{\Delta r_s}{r_s}+\left(\frac{\partial E}{\partial r_a}\frac{r_a}{E}\right)\frac{\Delta r_a}{r_a}+\left(\frac{\partial E}{\partial s}\frac{s}{E}\right)\frac{\Delta s}{s} \quad (12)$$

where the five terms in brackets quantify the relative sensitivity of E to change in R_n^*, D, r_s, r_a and s, respectively (that is, relative changes in E induced by relative changes in the forcing variables).

The Budyko model. The Budyko model describes the hydrologic partitioning as a functional balance between the atmospheric water supply (P) and demand (E_p) and a land-specific parameter (n) that modifies the steady-state hydrology–climate relationship at the mean annual scale[19,33]. Here, we adopted an analytical steady-state solution to the Budyko framework given by Choudhury[33]:

$$Q=P-E=P-\frac{PE_p}{(P^n+E_p^n)^{1/n}} \quad (13)$$

where P is the precipitation (mm yr^{-1}) and E is the actual evapotranspiration (mm yr^{-1}). n is a land-specific parameter that encodes all the influences other than the mean climate conditions (that is, P and E_p) and is fixed at $n=1.9$ in this study[19]. (Note that the discrepancies between Fig. 3b and Fig. 3e are improved when using a spatially varying n; that is, the value of n was calibrated against the CMIP5-modelled Q for each grid cell during the historical period 1861–1960 (Supplementary Fig. 8)).

PM-RC E_P model modified to account for atmospheric [CO_2]. Although not used in the paper, here we provide a modified formula to account for changing [CO_2] for the FAO-56 reference crop formula, provided as:

$$E_P=\frac{0.408sR_n^*+\gamma\frac{900}{T+273}uD}{s+\gamma\{1+u[0.34+2.4\times10^{-4}([CO_2]-300)]\}} \quad (14)$$

where the term $2.4\times10^{-4}([CO_2]-300)$ accounts for changing [CO_2] on r_s. The derivation of equation (14) is given in Supplementary Text 1 and a worked example of applying equation (14) is provided in Supplementary Table 2.

Data availability

The CMIP5 model outputs are available from the CMIP5 archive (http://cmip-pcmdi.llnl.gov/cmip5/).

References

31. Taylor, K. E., Stouffer, R. J. & Meehl, G. A. An overview of CMIP5 and the experiment design. *Bull. Am. Meteorol. Soc.* **93**, 485–498 (2012).
32. Jones, P. W. First- and second-order conservative remapping schemes for grids in spherical coordinates. *Mon. Weather Rev.* **127**, 2204–2210 (1999).
33. Choudhury, B. Evaluation of an empirical equation for annual evaporation using field observations and results from a biophysical model. *J. Hydrol.* **216**, 99–110 (1999).